ACS APPLIED MATERIALS & INTERFACES

Research Article

www.acsami.org

Transformation of $TiOF_2$ Cube to a Hollow Nanobox Assembly from Anatase TiO_2 Nanosheets with Exposed {001} Facets via Solvothermal Strategy

Ze'ai Huang, Zhouyou Wang, Kangle Lv,* Yang Zheng, and Kejian Deng

Key Laboratory of Catalysis and Materials Science of the State Ethnic Affairs Commission & Ministry of Education, South-Central University for Nationalities, Wuhan 430074, Hubei, P. R. China

Supporting Information

ABSTRACT: Hierarchical nanostructures have attracted increasing interest due to their exceptional properties and widespread potential applications. In this paper, anatase TiO_2 hollow nanoboxes (TiO_2–HNBs) are formed by assembly of nanosheets with exposed {001} facets by solvothermal treatment of $TiOF_2$ cubes in alcohols (*tert*-butanol and ethanol) at 180 °C. It was found that phase transformation of $TiOF_2$ to anatase TiO_2 begins at corners and edges of $TiOF_2$ cubes due to in situ hydrolysis of $TiOF_2$, where water was produced by dehydration of alcohol molecules. With extension the reaction time, TiO_2–HNB assemblies from nanosheets with exposed high-energy {001} facets were formed due to the steady inside–outside dissolution-recrystallization process. However, the resulting hierarchical TiO_2–HNBs are unstable, which can decompose to discrete high-energy TiO_2 nanosheets if the reaction time is further extended. The hierarchical TiO_2–HNBs show higher photocatalytic activity than discrete high-energy TiO_2 nanosheets and P25 TiO_2 due to the unique structures of TiO_2–HNBs.

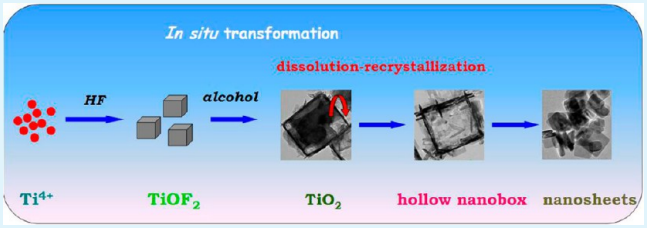

KEYWORDS: *titanium oxidifluoride, titanium dioxide, photocatalytic activity, hollow nanobox, hierarchical structure*

1. INTRODUCTION

Hierarchical nanostructures have attracted much attention due to their unique properties and potential practical applications.[1,2] Up to now, many hierarchical nanostructures have been reported, such as nanoleaves,[3] nanotubes,[4] hollow nanoparticles,[5] nanorattles[6] and even nanowebs.[7] Large fractions of void space in hollow structures has been successfully used to encapsulate and control release of sensitive materials such as drugs, cosmetics, and DNA. Likewise, the void space in hollow particles has been used to modulate refractive index, lower density, increase active area for catalysis, improve the particles' ability to withstand cyclic changes in volume, and to expand the array of imaging markers suitable for early detection of cancer.[1] Many studies also showed that TiO_2 hollow spheres perform much higher photocatalytic activity than solid spheres due to their stronger adsorption to substrates and/or higher light-harvesting ability.[5,6,8,9] Recently, our group has reported the synthesis of TiO_2 hollow microsphere assemblies from hollow nanoparticles with enhanced photocatalytic activity.[10] However, fabrication of hierarchical nanomaterials with complex structures still remains a great challenge.

As the most promising photocatalyst, anatase TiO_2 has been intensively investigated for the purpose of improving its photocatalytic performance.[11] Recently, much attention has been paid to fabrication of TiO_2 nanocrystals with exposed {001} facets due to their superior photocatalytic activity.[12−14] Using HF as a morphology controlling agent, an important breakthrough was made by Lu et al., who successfully synthesized TiO_2 single microcrystals with 47% {001} facets.[15] After that, many works have focused on the synthetic method of preparing TiO_2 nanocrystals exposed by {001} facets and the exploration of their applications in the utilization of solar energy.[16−18]

$TiOF_2$ cubes in sizes of submicro- or nanometers have been reported in the literature.[19−22] For example, Kuang[23] and Huang[20,21] et al. successfully synthesized cubic $TiOF_2$ with a uniform edge length through a solvothermal reaction method using tetrabutyl titanate (TBT), hydrofluoric acid (HF), and acetic acid (HAc) at 200 °C for 12 h.[23] However, the study of our group[14,24] and another report[22] showed that the photocatalytic activity of $TiOF_2$ was very poor. Considering that $TiOF_2$ can transform into anatase TiO_2 and fluoride ions should facilitate the formation of TiO_2 nanocrystals with exposed high reactive {001} facets, it is therefore anticipated the fabrication of TiO_2 hollow nanoboxes (TiO_2–HNBs) enclosed by high-energy TiO_2 nanocrystals via in situ phase transformation strategy (self-templated). TiO_2–HNBs, each enclosed by six single-crystalline TiO_2 plates exposed with highly reactive {001} facets, were obtained by Kuang et al. by calcining cubic $TiOF_2$ solid precursor at 500–600 °C for 2 h.[22] However, calcination of $TiOF_2$ at 500–600 °C for 2 h is highly energy-wasting. Hierarchical TiO_2–HNBs, enclosed by ordered arranged TiO_2

Received: June 13, 2013
Accepted: August 12, 2013
Published: August 12, 2013

   dx.doi.org/10.1021/am4023048 | ACS Appl. Mater. Interfaces 2013, 5, 8663–8669

nanorod arrays, were obtained by Huang et al. through hydrolysis of $TiOF_2$ cubes in basic solution (pH 11) via a template-engaged topotactic transformation process.[20] However, the prepared TiO_2–HNBs lost the exposure of high-energy {001} facets. How to transform $TiOF_2$ cubes to hierarchical TiO_2–HNBs using highly reactive {001} facets as building blocks at low temperature (less than 200 °C) still remains a great challenge.

In this paper, TiO_2–HNBs assembly from nanosheets with exposed high reactive {001} facets were successfully fabricated by in situ transformation of cubic $TiOF_2$ at 180 °C using alcohol as solvent. It was found that a small amount of water produced by dehydration of alcohols is of great importance on the hydrolysis of $TiOF_2$ and formation of TiO_2–HNBs. In this work, we report, for the first time, in situ transformation of $TiOF_2$ cubes to TiO_2–HNBs assembly from high-energy TiO_2 nanosheets via solvothermal strategy.

2. EXPERIMENTAL SECTION

2.1. Preparation of $TiOF_2$ Precursor. $TiOF_2$ precursor was prepared by a microwave-assisted synthetic strategy. Typically, 34.0 g TBT (0.1 mol) was dropwised into the mixture solution of 12.5 mL of HF (40 wt %, 0.25 mol) and 60.0 mL of HAc (1.0 mol) under magnetic stirring. After stirring for about 20 min, the obtained white suspensions were transferred to a Teflon-lined double-walled digestion vessel and heated at 200 °C for 60 min using a microwave digestion system (MDS-6, Sineo, Shanghai, China). After cooling to room temperature, the white precipitates were filtrated through a membrane filter (pore size, 0.45 μm) and rinsed with distilled ethanol and water until the pH value of the filtrate is about 7. The obtained white powders were collected and dried in a vacuum oven at 80 °C for 6 h.

2.2. Preparation of TiO_2–HNBs. TiO_2–HNBs were prepared through a solvothermal strategy using alcohol as solvent. Specifically, 2.0 g of the as-prepared $TiOF_2$ precursor were mixed with 40 mL *tert*-butanol and transferred into a Teflon-lined autoclave after ultrasonic dispersion for 10 min. Then, the reactants were heated at 180 °C for a certain time (1–10 h) in an oven. After cooling down naturally to room temperature, the products were filtrated through a membrane filter (pore size 0.45 μm). To eliminate the surface adsorbed fluoride ions, the precipitate was washed by 0.1 M NaOH,[14] followed by distilled water until the pH value of the filtrate is about 7. The resulted white cake was dried in a vacuum oven at 80 °C for 6 h. The obtained samples were labeled as T*x*, where *x* represents the time of heat treatment (Table 1). For example, the T4 sample means the photocatalyst was obtained by heat treatment $TiOF_2$ precursor in *tert*-butanol at 180 °C for 4 h. T0 represents precursor $TiOF_2$.

Table 1. Physical Properties of the Photocatalysts

sample	phase[a]	S_{BET} (m^2/g)	pore volume (cm^3/g)	average pore size (nm)
T0	$TiOF_2$	8.2	0.019	9.2
T1	$TiOF_2$	8.0	0.016	7.8
T2	$TiOF_2$/A-TiO_2	46.0	0.13	11.2
T3	A-TiO_2	56.0	0.22	16.8
T4	A-TiO_2	66.4	0.28	17.1
T5	A-TiO_2	51.8	0.28	21.3
T10	A-TiO_2	41.0	0.23	22.2

[a]A-TiO_2 means anatase TiO_2.

2.3. Characterization. The X-ray diffraction (XRD) patterns of the samples were obtained on a D8 advance X-ray diffractometer (Germany Bruker) using Cu Kα radiation at a scan rate (2θ) of 0.05 s^{-1}. The voltage and applied current were 40 kV and 80 mA, respectively. The morphology of the photocatalyst was observed on a transmission electron microscopy (TEM) (Tecnai G20, USA) using an acceleration voltage of 200 kV and a field emission scanning electron microscope (SEM) (Hitach, Japan) with an acceleration voltage of 20 kV, respectively. Nitrogen adsorption–desorption isotherms were obtained on an ASAP 2020 (Micromeritic Instruments, USA) nitrogen adsorption apparatus. All the samples were degassed at 120 °C prior to Brunauer–Emmett–Teller (BET) measurements. The BET specific surface area (S_{BET}) was determined by a multipoint BET method using the adsorption data in the relative pressure P/P_0 range of 0.05–0.30. The desorption isotherm was used to determine the pore size distribution by using the Barret–Joyner–Halenda (BJH) method. The nitrogen adsorption volume at P/P_0 = 0.994 was used to determine the pore volume and average pore size.

2.4. Evaluation of the Photocatalytic Activity. The photocatalytic activity of the photocatalyst was evaluated by a photoluminescence (PL) technique using coumarin as a probe molecule, which readily reacted with ·OH radicals to produce highly fluorescent product, 7-hydroxycoumarin (Scheme 1).[14,25] The suspensions of TiO_2 (1.0 g/L) containing coumarin (0.5 mmol/L) were mixed under magnetic stirring and, then, shaken overnight. At given intervals of irradiation, small aliquots were withdrawn by a syringe and filtered through a membrane (pore size 0.45 μm). The solution after filtration through a 0.45 μm membrane filter was analyzed on a Hitachi F-7000 fluorescence spectrophotometer by the excitation with the wavelength of 332 nm.

Scheme 1. Formation of 7-Hydroxycoumarin (Strong Fluorescent Molecule) in the Reaction of Coumarin (Weak Fluorescent Molecule) with Hydroxyl Radicals

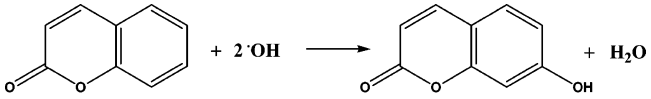

3. RESULTS AND DISCUSSION

3.1. Microwave-Assisted Synthesis $TiOF_2$ Precursor. It was reported that $TiOF_2$ can be synthesized by heat treatment of the mixed solution of TBT, HF, and HAc at 200 °C for 12 h.[20] However, this conventional heating method is time-consuming. Microwave-assisted heating can reduce the time required for the synthesis and increase the crystallinity of the product.[16] Solvents which are polar in nature have a good potential to adsorb microwaves and convert them to thermal energy, thus accelerating the reactions as compared to results obtained using conventional heating. Therefore, we try to synthesize $TiOF_2$ via a microwave-assisted strategy. After microwave-assisted heating at 200 °C for 60 min, it was found that pure phase $TiOF_2$ was successfully synthesized (T0 sample in Figure 1a). SEM and TEM images

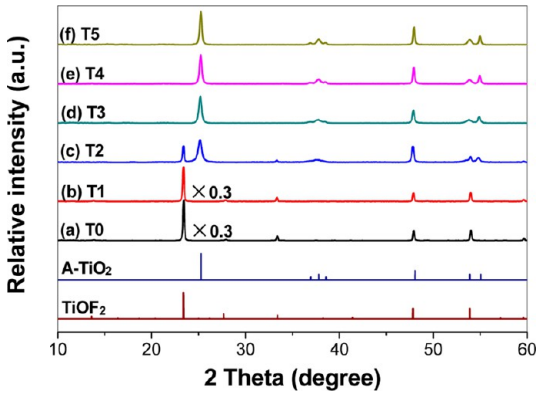

Figure 1. XRD patterns of the samples, together with the expected diffraction peaks for $TiOF_2$ and anatase TiO_2 (A-TiO_2).

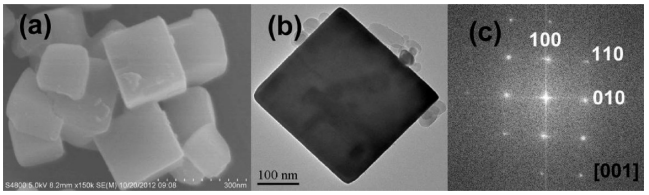

Figure 2. SEM (a) and TEM (b) characterization of $TiOF_2$ cubes. (c) Corresponding SEAD pattern of a single $TiOF_2$ cube shown in part b.

show that $TiOF_2$ crystals are cubes with a side length of ca. 200−300 nm (Figure 2a and b). The corresponding selected area electron diffraction (SAED) pattern of a single $TiOF_2$ crystal confirms the typical *Pm*3*m* structure of $TiOF_2$ precursor (Figure 2b and c).[19] The experimental results infer that $TiOF_2$ can be successfully synthesized by a microwave-assisted strategy, which is more efficient than conventional heating method.

3.2. Phase Transformation and Shape Evolution of $TiOF_2$ Cubes in TBA. Hydrolysis of $TiOF_2$ precursor is necessary for phase transformation of $TiOF_2$ to TiO_2. To verify the effect of water on this phase transformation, solvothermal treatment of $TiOF_2$ in anhydrous solvent (CCl_4) and aqueous solution were performed for comparison. It was found that the morphology of $TiOF_2$ was unchanged (Supporting Information Figure S1) and no phase transformation was observed (not shown here) in anhydrous CCl_4 solvent even with treatment of $TiOF_2$ precursor at 180 °C for 24 h. However, the XRD pattern shows that pure anatase TiO_2 was obtained with hydrothermal treatment of $TiOF_2$ precursor at 180 °C for 1 h (Supporting Information Figure S2), reflecting the importance of water for phase transformation of $TiOF_2$ to TiO_2. TEM image shows that a mixture of TiO_2 nanoparticles and a small amount of TiO_2−HNBs assembly from nanoparticles were obtained (Supporting Information Figure S3a and b) after hydrothermal reaction for 1 h. The obtained TiO_2−HNBs are unstable and can collapse to nanoparticles if the reaction is extended to 2−5 h (Supporting Information Figure S3c and d). This infers that quick hydrolysis of $TiOF_2$ in aqueous solution is harmful for self-templated formation of TiO_2−HNBs due to fast mass transfer in shape evolution (eq 1).

$$TiOF_2 + H_2O = TiO_2 + 2HF \quad (1)$$

A conclusion can be drawn from the above experiments that water is necessary, but it should be in low concentration in self-templated fabrication of TiO_2−HNBs. Furthermore, too much water results in a low F^- concentration, also not good for the exposure high reactive {001} facets for TiO_2 nanocrystal building blocks. Considering that a small amount of water can be obtained by heat treatment of alcohol (dehydration), solvothermal treating of $TiOF_2$ in *tert*-butanol (TBA) and ethanol was therefore systematically studied.

Figure 1 shows the effect of reaction time on the phase transformation of $TiOF_2$ precursor in TBA solvent at 180 °C. As for the precursor T0, all the diffraction peaks corresponding to $TiOF_2$ (JCPDS No. 08-0060) were observed and no peak of any anatase TiO_2 phase exists, indicating the pure phase of the precursor. The broad peak at $2\theta = 23.4°$ corresponds to the (100) plane diffraction of $TiOF_2$ (Figure 1a).[19] However, when the reaction time is extended from 0 to 3 h, the peak at $2\theta = 23.4°$ gradually disappears, reflecting that hydrolysis of $TiOF_2$ begins possibly due to the in situ production the small amount of water by dehydration of TBA. Meanwhile, a broad peak at $2\theta = 25.3°$, corresponding to the diffraction peak of (101) plane of anatase TiO_2 (JCPDS No. 21-1272),[26] is formed for T2 sample (Figure 1c), indicating the mixed phases of T2 sample. The mass ratios of $TiOF_2$ and anatase TiO_2 for T2 sample were calculated to be 15% and 85%, respectively. Phase transformation from $TiOF_2$ to anatase TiO_2 is completed after reaction for 3 h (Figure 1d).

Further observation shows that increasing the reaction from 3 to 5 h, XRD peak intensities of anatase become stronger and the width of XRD diffraction peaks of anatase becomes narrower, indicating the formation of highly crystalline TiO_2 crystals, which is because the dissolution-recrystallization of TiO_2 nanocrystals in the presence of fluoride ions. It was reported that the presence of fluoride ions at low pH accelerates TiO_2 crystallization and growth due to rapid in situ dissolution-recrystallization, which reduces the numbers of defects and impurities in the TiO_2 lattice (eqs 2 and 3).[5,14]

$$4H^+ + TiO_2 + 6F^- \rightarrow TiF_6^{2-} + 2H_2O \quad \text{(dissolution)} \quad (2)$$

$$TiF_6^{2-} + 2H_2O \rightarrow 4H^+ + TiO_2 + 6F^- \quad \text{(recrystallization)} \quad (3)$$

Figure 3 shows the morphology evolution of $TiOF_2$ precursor in solvothermal reaction. The shape of $TiOF_2$ cubes becomes

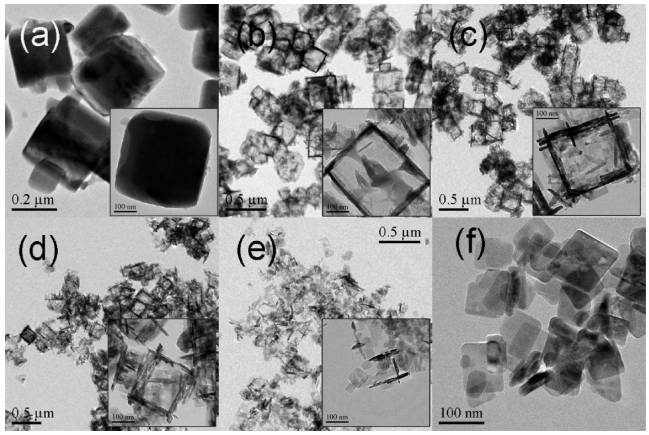

Figure 3. TEM images of the photocatalysts obtained by solvothermal treatment of $TiOF_2$ precursor in TBA at 180 °C for 1 h (T1, a), 2 h (T2, b), 3 h (T3, c), 4 h (T4, d), 5 h (T5, e) and 10 h (T10, f), respectively.

not so regular after reaction for 1 h (T1) when compared with that of precursor T0 sample (Figures 2 and 3a). This is possibly due to the hydrolysis of $TiOF_2$ (eq 1), and the dissolution begins from the edges and corners of $TiOF_2$ cubes (inset of Figure 3a). Generally speaking, the atoms at corners or edges of crystals are more active than those in other parts of the cube because of their special microenvironment.

Figure 3b shows the TEM image of T2 sample. It can be seen that the morphology of T2 changes to hollow nanoboxes with side length of ca. 200−300 nm, which is the same size as that of $TiOF_2$ precursor, reflecting that the hollow nanoboxes were formed through in situ transformation of $TiOF_2$ precursor (self-templated). Careful viewing shows that the core ($TiOF_2$) in hollow nanoboxes was not completely dissolved (inset of Figure 3b), in accordance with the $TiOF_2$/A-TiO_2 mixed phase structure of T2 sample (Figure 1c). When the reaction time is extended to 3−4 h, phase transformation from $TiOF_2$ to anatase TiO_2 completes, resulting in the production of TiO_2−HNBs (Figure 3c and d). However, almost only nanosheets can be observed if further increase in the reaction time to 5 h

(Figure 3e), possibly due to the collapse of TiO_2–HNBs because of the further etching by fluoride ions (eqs 2 and 3). Figure 3f shows the TEM image of T10 sample, the sheet-like structure of T10 sample further confirming the complete decomposition of TiO_2–HNBs during solvothermal reaction process.

To get more information about the formed TiO_2–HNBs and nanosheets, high-resolution TEM (HRTEM) was used to analyze the structures of the samples. Figure 4b shows the HRTEM image of T4 sample originated from the corner of a TiO_2–HNB (Figure 4a). From the lattice fringes of 0.235 nm, corresponding to the (001) planes of anatase TiO_2, and the angle of ca. 68.3°, which is consistent with the interfacial angle between (001) and (101), it is safe to conclude that TiO_2–HNBs are in fact assembly from TiO_2 nanosheets with exposed high reactive {001} facets. The obtained TiO_2 nanosheets after the collapse of TiO_2–HNBs were also exposed with dominant {001} facets (Figure 4c and d for T10 sample).

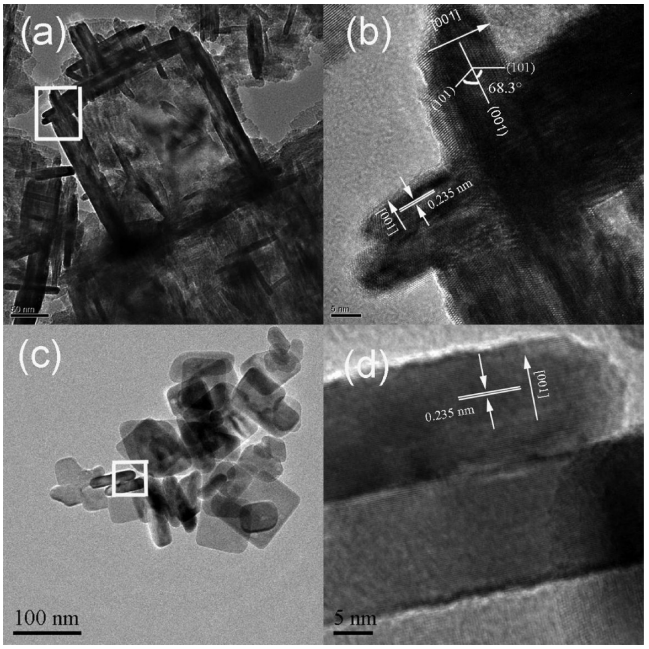

Figure 4. TEM images of T4 (a) and T10 (c) samples. (b and d) Corresponding HR-TEM images of the parts of T4 and T10 samples shown in parts a and c, respectively.

Consistent with the results from TEM images, the shape evolution of $TiOF_2$ precursor from cubes (Figure 5a) to a hollow nanobox assembly from nanosheets (Figure 5b–e) and discrete nanosheets (Figure 5f) can also be clearly seen from the corresponding SEM images.

3.3. Nitrogen Adsorption. Figure 6 shows nitrogen adsorption–desorption isotherms and the corresponding pore size distribution curves of the photocatalysts. It can be seen that T0 sample (precursor) shows poor nitrogen adsorption due to it is large particle size, reflecting a small BET specific surface area (only 8.2 $m^2\ g^{-1}$ for $TiOF_2$ precursor).[14,24,27] When extension the reaction time to 4 h, the adsorption isotherm obviously shifts upward, indicating an increase BET surface area (66.4 $m^2\ g^{-1}$ for T4 sample), which is ascribed to the formation of TiO_2–HNBs (Figures 3 and 5). However, further increase in the reaction time to 10 h, the adsorption isotherm begins to shift downward due to enhanced crystallization of TiO_2 nanosheets, which infers a decreased BET surface area (41.0 $m^2\ g^{-1}$ for T10).

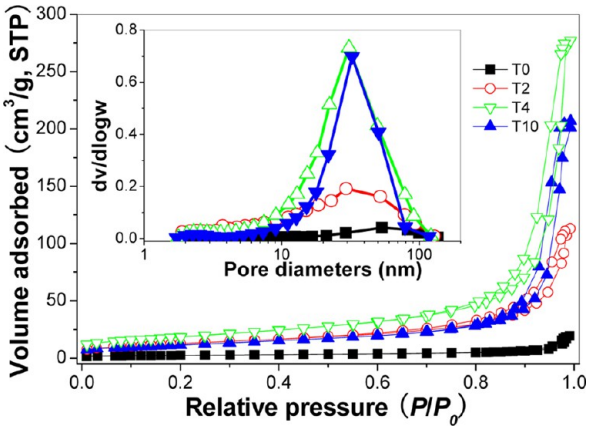

Figure 6. Nitrogen adsorption–desorption isotherms and the corresponding pore size distribution curves (inset) of the photocatalysts.

The shape of the isotherm for TiO_2–HNBs (T4 as an example) is type IV with one hysteresis loop at a relative pressure range of 0.8–1.0, indicating the presence of mesopores.[14,17] Typically, the shape of the hysteresis loop for T4 (TiO_2–HNBs) is H3, suggesting narrow slit-shaped pores that are generally associated with platelike particles, which agrees well with their sheetlike morphology (Figure 3d).[14]

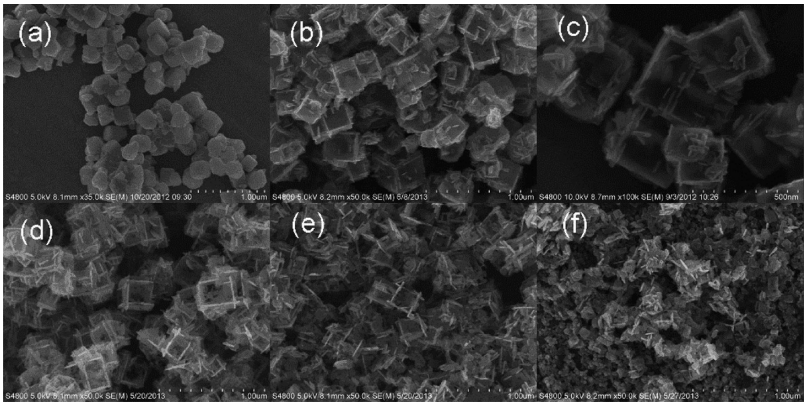

Figure 5. SEM images of T1 (a), T2 (b and c), T3 (d), T4 (e), and T5 (f) samples, respectively.

Table 1 summarizes the physical properties of the photocatalysts. It can be seen that the BET specific surface areas and pore volumes of the photocatalysts increase first and then decrease due to shape evolution of the sample from solid cubes to hollow nanoboxes and discrete nanosheets. The T4 sample has the largest BET surface area (66.4 $m^2 g^{-1}$) and pore volume (0.28 $cm^3 g^{-1}$), which should benefit its photocatalytic activity.

3.4. Photocatalytic Activity. It has been proven that several weakly luminescent molecules, such as terephthalic acid[25] and coumarin[10,14] can produce strongly luminescent compounds when reacted with ·OH radicals, and these molecules can be applied for evaluation of the relative photocatalytic activity of the photocatalysts. Herein coumarin is used as a probe to evaluate the photocatalytic activity of the photocatalysts (Scheme 1).

The inset of Figure 7A shows the typical PL spectral changes observed during illumination of the suspensions of T4 sample

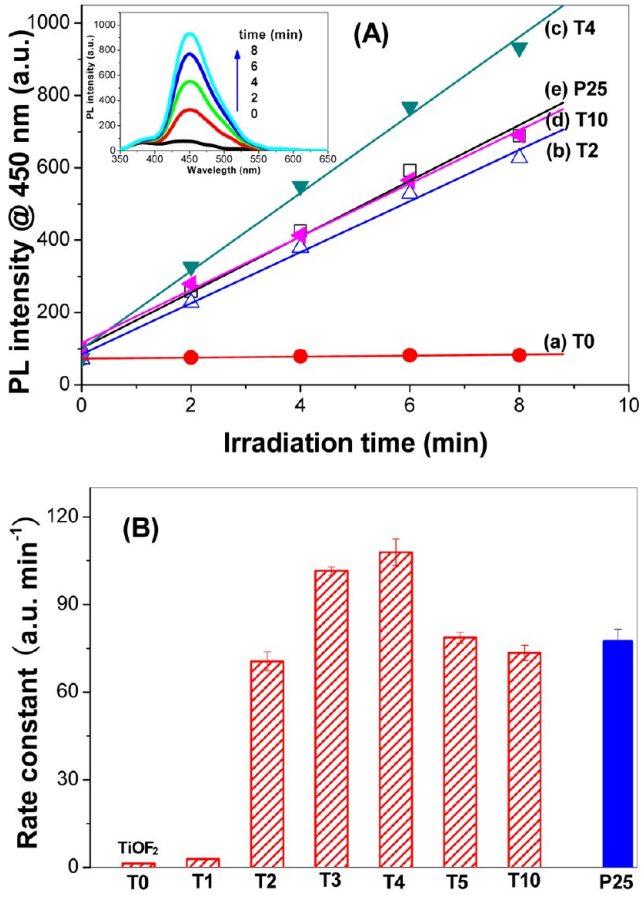

Figure 7. Time dependence of the induced photoluminescence intensity at 450 nm of the photocatalysts (A) and comparison of the rate constants (B) for sample T4. (inset) Photoluminescence spectral changes observed during illumination of the suspensions of T4 TiO_2–HNBs.

(TiO_2–HNBs). It is observed that the PL intensity of photogenerated 7-hydroxycoumarin at 450 nm (excited at 332 nm) increases with irradiation time. Figure 7A records the time course of the PL intensity of 7-hydroxycoumarin at 450 nm during the irradiation of the photocatalysts. It is clearly seen that the PL intensity at 450 nm increases linearly against the irradiation time. This leads to a conclusion that the generation of fluorescent 7-hydroxycoumarin is linearly proportional to illumination time, obeying a pseudo-zero-order reaction rate equation in kinetics. The slopes for the curve of PL intensity versus illumination time (rate constant), which represent the photocatalytic activity of the photocatalysts, increase first and then decease with increasing the solvothermal reaction time in preparation of the photocatalysts. $TiOF_2$ precursor shows poor photocatalytic activity (rate constant of only 1.36), which is consistent with our previous report.[14,24] However, the T4 sample shows the highest photocatalytic activity among all the photocatalysts (rate constant of 107.9), which is 40% higher than that of Degussa P25 TiO_2 (rate constant of 77.2).

According to XPS characterization results (Supporting Information Figure S6), surface adsorbed fluoride ions (binding energy of 684.0 eV) were detected on the surface of the photocatalysts. However, no signal of F^- in lattice of TiO_2 (binding energy of 688.5 eV) is found for all TiO_2–HNBs photocatalysts.[14] Therefore, the F-doping of TiO_2–HNBs can be excluded. This is not difficult to understand because, on the one hand, the hydrothermal environment can accelerate crystallization of TiO_2 due to the in situ dissolution–recrystallization process, resulting in the reduction of the number of defects and impurity in TiO_2 nanocrystals (eqs 2 and 3). The actual amount of fluorine detected by XPS on the surface of $TiOF_2$ precursor (T0) was 1.88 at % . However, the fluoride adsorbed on the surface of TiO_2–HNBs can be neglected (0.12 at %).

According to diffuse reflectance spectra (DRS) shown in Supporting Information Figure S7, the band gap of TiO_2–HNBs (T4) was calculated to be 3.23 eV, which is larger than that of P25 TiO_2 (3.14 eV). Therefore, the F-doping of TiO_2–HNBs, which will narrow the band gap of TiO_2, can also be excluded. Comparing the DRS between T4 and T10 samples, it can be seen that TiO_2–HNBs (T4) show stronger absorbance due to its unique structure, which can offer an improved catalytic activity.

There are many reports by others[15,17] and our work[14,16] about the effect of exposed {001} facets on the enhanced photocatalytic activity of TiO_2 nanocrystals. As a commercial photocatalyst, the high photocatalytic activity of P25 is ascribed to its good crystallization and anatase–rutile mixed phase, which was prepared by calcination at high temperature (about 600 °C). Although the T4 sample was prepared at lower temperature (only 180 °C), it shows higher photocatalytic activity than P25 due to the exposure of {001} facets and hollow structures. The high specific surface area (66.4 m^2/g for T4) should also benefit the photocatalytic activity of TiO_2–HNBs.

Further experiments also indicate that the as-prepared TiO_2–HNBs can be more readily separated from the slurry system by filtration or sedimentation after photocatalytic reaction and reused than the corresponding nanosized photocatalytic powders due to their large weight, weak Brownian motion, and good mobility.

3.5. Phase Transformation and Shape Evolution in Ethanol. To further confirm the effect of solvent on the formation of TiO_2–HNBs, solvothermal treatment of $TiOF_2$ precursor was also performed in ethanol. Similar results as in TBA were obtained. However, the phase transformation from $TiOF_2$ to anatase TiO_2 in ethanol is much slower than in TBA (Figures 1 and 8). After reaction at 180 °C for 5 h, no phase transformation from $TiOF_2$ to anatase TiO_2 can be observed. Pure anatase TiO_2 phase was obtained when extension the reaction time to 10 h. Similar to the results in TBA, the evolution of the shapes, from cubes to hollow nanoboxes and discrete nanosheets, was also observed in ethanol (Figure 9). It can also be clearly seen from Figure 9d that TiO_2–HNBs begins to form at the edges of the precursor (self-templated in situ transformation).

dx.doi.org/10.1021/am4023048 | ACS Appl. Mater. Interfaces 2013, 5, 8663–8669

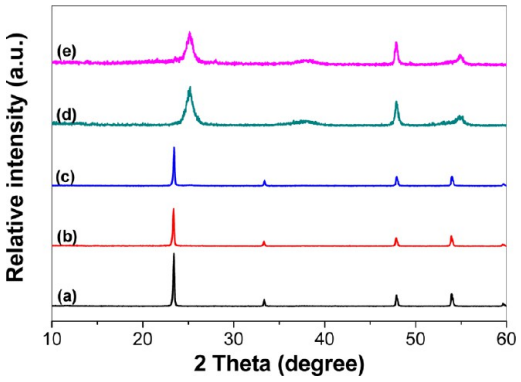

Figure 8. XRD patterns of the samples after solvothermal treatment of $TiOF_2$ precursor (T0) in ethanol at 180 °C for 1 h (a), 2 h (b), 5 h (c), 10 h (d), and 24 h (e), respectively.

3.6. Formation Mechanism of TiO_2–HNBs. To elucidate the formation mechanism of TiO_2–HNBs, organics produced in TBA or ethanol after solvothermal treatment of $TiOF_2$ precursor were detected by GC-MS. It was found that most of these organics were alkenes and ester (Supporting Information Figures S4 and S5), which should come from the dehydration of the corresponding alcohol. Our study showed that water is necessary for the successful transformation of $TiOF_2$ cubes to anatase TiO_2–HNBs. However, the contents of water should be low (Supporting Information Figures S1–S3). Therefore, the dehydration of alcohol during solvothermal treatment is of great importance for the hydrolysis of cubic $TiOF_2$ precursor, which results in the in situ transformation of $TiOF_2$ to anatase TiO_2 nanocrystals (eqs 4 and 5).

$$\text{alcohol} \xrightarrow{\text{dehydration}} \text{alkene (ester)} + H_2O \quad (4)$$

$$TiOF_2 + H_2O = TiO_2\ (\text{anatase}) + 2HF \quad (\text{in situ transformation}) \quad (5)$$

With further increase in the reaction time, more water was produced. The steady dissolution of $TiOF_2$ at the corner and edge of the cubes, together with the recrystallization of anatase TiO_2 on the surface (inside–outside mass transfer), results in the formation of TiO_2–HNBs (eqs 6). Since dehydration reaction of TBA is easier than that of ethanol (eq 4), it is not surprising that the dissolution of $TiOF_2$ cubes in TBA, forming anatase TiO_2–HNBs, is much quicker than that in ethanol under other identical conditions.

$$TiOF_2 + 2H^+ + 4F^- = TiF_6^{2-} + H_2O \quad (\text{dissolution}) \quad (6a)$$

$$TiOF_6^{2-} + H_2O = TiO_2\ (\text{anatase}) + 2H^+ + 6F^- \quad (\text{recrystallization}) \quad (6b)$$

It has been reported that high energy {001} facets can be exposed in the presence of fluoride ions (shape-directing reagent). Therefore, TiO_2–HNBs, assembly from anatase TiO_2 nanosheets with dominant high reactive {001} facets, were successfully fabricated in this system. However, over growth results in the collapse of TiO_2–HNBs, forming discrete high-energy TiO_2 nanosheets due to the etching of fluoride ions in solution. The proposed formation mechanism was summarized in Figure 10.

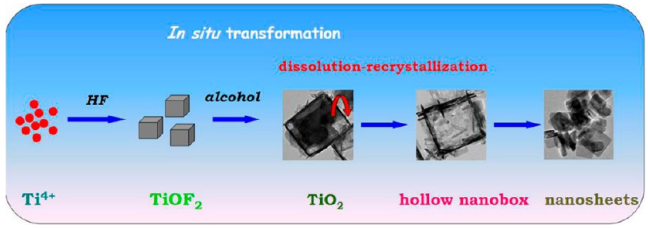

Figure 10. Proposed mechanism for the formation of anatase TiO_2 hollow nanoboxes.

4. CONCLUSIONS

The precursor of $TiOF_2$ can be successfully synthesized by a microwave-assisted method, which is more efficient than a conventional heating method. TiO_2 hollow nanoboxes enclosed by high reactive anatase TiO_2 nanosheets were also successfully prepared using $TiOF_2$ cubes as precursor via solvothermal strategy. The production of water by dehydration of alcohol is of great importance for the hydrolysis of $TiOF_2$, forming TiO_2–HNBs followed by in situ transformation and dissolution-recrystallization process. The prepared TiO_2–HNBs show high photocatalytic activity due to their special structures. The proposed route for the preparation of TiO_2–HNBs has the merits of being simple, reproducible, and easy to scale-up, which is expected to be widely used in photocatalysis, catalysis, electrochemistry, separation, purification, drug delivery, and so on.

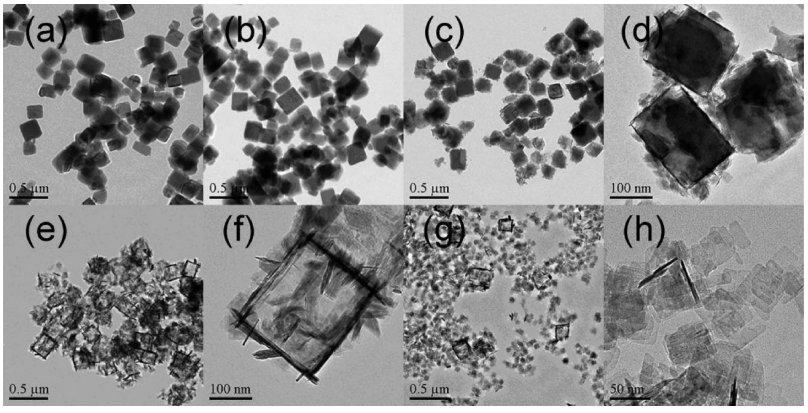

Figure 9. TEM images of the photocatalysts after solvothermal treatment of $TiOF_2$ (T0) in ethanol at 180 °C for 1 h (a), 2 h (b), 5 h (c and d), 10 h (e and f), and 24 h (g and h), respectively.

dx.doi.org/10.1021/am4023048 | ACS Appl. Mater. Interfaces 2013, 5, 8663–8669

■ ASSOCIATED CONTENT

Supporting Information

TEM image of the sample prepared by solvothermal treatment of $TiOF_2$ precursor in carbon tetrachloride (CCl_4) at 180 °C for 24 h, XRD patterns of the samples after hydrothermal treatment of $TiOF_2$ precursor in water at 180 °C, TEM images of the samples after hydrothermal treatment of $TiOF_2$ (T0) in water at 180 °C, detailed procedure for detection of organics in solvent by GC-MS, and UV−vis diffuse reflectance spectra and XPS characterization of the photocatalysts. This material is available free of charge via the Internet at http://pubs.acs.org.

■ AUTHOR INFORMATION

Corresponding Author

*Tel: +86-27-67842752. Fax: +86-27-67842752. E-mail: lvkangle@mail.scuec.edu.cn.

Notes

The authors declare no competing financial interest.

■ ACKNOWLEDGMENTS

This work was supported by the Program for New Century Excellent Talents in University (NCET-12-0668), National Natural Science Foundation of China (20977114 and 21373275), and Natural Science Foundation of Hubei Province (2011CDA107).

■ REFERENCES

(1) Lou, X. W.; Archer, L. A.; Yang, Z. C. *Adv. Mater.* **2008**, *20*, 3987−4019.
(2) Yu, J. G.; Su, Y. R.; Cheng, B. *Adv. Funct. Mater.* **2007**, *17*, 1984−1990.
(3) Wang, L.; Li, H. L.; Tian, J. Q.; Sun, X. P. *ACS Appl. Mater. Interfaces* **2010**, *2*, 2987−2991.
(4) Sun, J.; Yan, X.; Lv, K. L.; Sun, S.; Deng, K. J.; Du, D. Y. *J. Mol. Catal. A: Chem.* **2013**, *367*, 31−37.
(5) Lv, K. L.; Yu, J. G.; Fan, J. J.; Jaroniec, M. *CrystEngComm* **2011**, *14*, 7044−7048.
(6) Li, H. X.; Bian, Z. F.; Zhu, J.; Zhang, D. Q.; Li, G. S.; Huo, Y. N.; Li, H.; Lu, Y. F. *J. Am. Chem. Soc.* **2007**, *129*, 8406−8407.
(7) Wang, H. T.; Wu, J. C.; Shen, Y. Q.; Li, G. P.; Zhang, Z.; Xing, G. Z.; Guo, D. L.; Wang, D. D.; Dong, Z. L.; Wu, T. *J. Am. Chem. Soc.* **2010**, *132*, 15875−15877.
(8) Li, X. F.; Lv, K. L.; Deng, K. J.; Tang, J. F.; Su, R.; Sun, J.; Chen, L. Q. *Mater. Sci. Eng., B* **2009**, *158*, 40−47.
(9) Liu, S. W.; Yu, J. G.; Mann, S. *Nanotechnology* **2009**, *20*, 325606.
(10) Cai, J. H.; Wang, Z. Y.; Lv, K. L.; Zheng, Y.; Yu, J. G.; Li, M. *RSC Adv.* **2013**, *3*, 15273−15281.
(11) Chen, X. B.; Shen, S. H.; Guo, L. J.; Mao, S. S. *Chem. Rev.* **2010**, *110*, 6503−6570.
(12) Liu, S. W.; Yu, J. G.; Jaroniec, M. *Chem. Mater.* **2011**, *23*, 4085−4093.
(13) Li, H. M.; Zeng, Y. S.; Huang, T. C.; Piao, L. Y.; Yan, Z. J.; Liu, M. *Chem.—Eur. J.* **2012**, *18*, 7525−7532.
(14) Wang, Z. Y.; Lv, K. L.; Wang, G. H.; Deng, K. J.; Tang, D. G. *Appl. Catal., B* **2010**, *100*, 378−385.
(15) Yang, H. G.; Sun, C. H.; Qiao, S. Z.; Zou, J.; Liu, G.; Smith, S. C.; Cheng, H. M.; Lu, G. Q. *Nature* **2008**, *453*, 638−641.
(16) Zheng, Y.; Lv, K. L.; Wang, Z. Y.; Deng, K. J.; Li, M. *J. Mol. Catal. A: Chem.* **2012**, *356*, 137−143.
(17) Yu, J. G.; Qi, L. F.; Jaroniec, M. *J. Phys. Chem. C* **2010**, *114*, 13118−13125.
(18) Wen, C. Z.; Zhou, J. Z.; Jiang, H. B.; Hu, Q. H.; Qiao, S. Z.; Yang, H. G. *Chem. Commun.* **2011**, *47*, 4400−4402.
(19) Chen, L.; Shen, L. F.; Nie, P.; Zhang, X. G.; Li, H. S. *Electrochim. Acta* **2012**, *62*, 408−415.
(20) Wang, Z. Y.; Huang, B. B.; Dai, Y.; Zhang, X. Y.; Qin, X. Y.; Li, Z.; Zheng, Z. K.; Cheng, H. F.; Guo, L. W. *CrystEngComm* **2012**, *14*, 4578−4581.
(21) Wang, Z. Y.; Huang, B. B.; Dai, Y.; Zhu, X. L.; Liu, Y. Y.; Zhang, X. Y.; Qin, X. Y. *CrystEngComm* **2013**, *15*, 3436−3441.
(22) Wen, C. Z.; Hu, Q. H.; Guo, Y. N.; Gong, X. Q.; Qiao, S. Z.; Yang, H. G. *Chem. Commun.* **2011**, *47*, 6138−6140.
(23) Xie, S. F.; Han, X. G.; Kuang, Q.; Fu, J.; Zhang, L.; Xie, Z. X.; Zheng, L. S. *Chem. Commun.* **2011**, *47*, 6722−6724.
(24) Lv, K. L.; Yu, J. G.; Cui, L. Z.; Chen, S. L.; Li, M. *J. Alloys Compd.* **2011**, *509*, 4557−4562.
(25) Lv, K. L.; Yu, J. G.; Deng, K. J.; Li, X. H.; Li, M. *J. Phys. Chem. Solid* **2010**, *71*, 519−522.
(26) Lv, K. L.; Li, X. F.; Deng, K. J.; Sun, J.; Li, X. H.; Li, M. *Appl. Catal., B* **2010**, *95*, 383−392.
(27) Zhu, J.; Zhang, D. Q.; Bian, Z. F.; Li, G. S.; Huo, Y. N.; Lu, Y. F.; Li, H. X. *Chem. Commun.* **2009**, 5394−5396.